Orbital-Angular-Momentum Quantum State Transformation Via a Nonlinear Process

Zhantong Qi,[1] Yiwen Huang,[1] Chuanyi Lu,[1] Fengchao Ni,[1] Yuanhua Li,[1,2,*] Yuanlin Zheng[1,3] and Xianfeng Chen[1,3,4,†]

[1] *State Key Laboratory of Advanced Optical Communication Systems and Networks, School of Physics and Astronomy, Shanghai Jiao Tong University, Shanghai 200240, China*
[2] *Department of Physics, Jiangxi Normal University, Nanchang 330022, China*
[3] *Shanghai Research Center for Quantum Sciences, Shanghai 201315, China*
[4] *Collaborative Innovation Center of Light Manipulation and Applications, Shandong Normal University, Jinan 250358, China*

Orbital-angular-momentum- (OAM) based photonic nonlinear interfaces, such as the nonlinear manipulation of a single-photon OAM state between the communication wavelength for entanglement distribution and the near-visible wavelength for quantum memories. Here, we experimentally demonstrate this kind of quantum state transformation for simultaneously adjusting the weight of the spatial OAM modes and operating the wavelength of single photons by effectively cascading the frequency conversion and electro-optical (EO) polarization coupling in a periodically poled lithium niobate crystal. The fidelity of the OAM state is measured to be higher than 95% before and after the frequency conversion. The results show that the OAM state of single photons can be modulated on demand by applying a transverse electric field across the nonlinear crystal. Our work demonstrates the integration and high performance of our proposed transformation interface, and paves a route toward connecting different remote nodes based on quantum memories in a large-scale OAM-encoded quantum network.

I. INTRODUCTION

Quantum relay network based on quantum entanglement is a useful choice for realizing large-scale quantum communication network [1,2]. Quantum state modulation is a promising technique for fundamental physics research, which is closely related to quantum relay switches, and quantum storage and processing of quantum states. To date, optical orbital-angular-momentum (OAM) modes, one of the foundations of spatial modes, have become a popular choice for quantum information experiments [3,4]. Since OAM single photons carry a unique phase intensity profile and multiple modes of operation, efforts to stimulate various quantum communication tasks [5–7] are increasing, such as quantum key distribution, quantum teleportation, entanglement swapping, etc. Establishing connections between different quantum systems to transmit information requires some basic components [8,9], such as quantum memory, relay nodes, quantum processors, etc. In order to realize the functions of these components, different physical systems usually work at different wavelengths. To

connect these systems, it is necessary to establish a wavelength connection such as a frequency converter, which can effectively realize the manipulation and wavelength conversion of photonic states [10–12]. Such frequency converters can be implemented using nonlinear crystals for second-order nonlinear processes [13–16]. In addition, great advances have been made in the cascade process [17,18] of frequency conversion and electro-optical (EO) polarization coupling, which have a broad range of applications in the control of OAM superposition states and the nonlinear optical interaction [19,20]. However, the electrical nonlinear modulation of OAM quantum states is useful for constructing the communication nodes in the quantum communication. At the same time, the traditional quantum state electrical manipulation and frequency-conversion process need to be carried out in the Mach-Zehnder interferometer (MZI) and the nonlinear crystal, respectively. Experimental demonstration of the electromanipulation is badly required, while combining integration and independence. Here, we demonstrate the nonlinear quantum state transformation for a quantum repeater network with the cascaded sum-frequency generation (SFG) and EO polarization coupling of OAM single photons in a periodically polarized lithium niobate (PPLN) crystal. By using input

*lyhua1984@jxnu.edu.cn
†xfchen@sjtu.edu.cn

photons with different OAM in orthogonal polarization components, we manage to adjust the weight of the spatial modes of the generated photons. The cascade process can be efficiently and conveniently balanced by applying an external electric field, realizing the superposition of quantum states with different OAM modes. The structure of the PPLN provides a general solution for combining optical spin-orbit coupling with nonlinear optics [21], and simultaneously enhances both the up-conversion efficiency and EO effect of OAM quantum states, resulting in better tunable performance. Through the cascade effect, we realize the OAM states' modulation on a single PPLN and convert the photons in the communication band to the storage band, which reduces the complexity of the experiment and makes the whole device more independent and stable. Furthermore, we clearly demonstrate that the transformation of different OAM quantum states maintains high fidelity during the conversion. In routing-based quantum networks, a single photons with a nonlinear process manage to convert the communication wavelength to the storage wavelength to realize the connection of two remote nodes. This holds more promise for practical applications of quantum storage and a quantum repeater in quantum networks.

II. THEORY

Under the effect of the second-order nonlinear of the crystal, quantum frequency conversion can be realized by SFG, in which the annihilation of a strong pump photon (ω_p) and a weak signal photon (ω_s) produce a SFG photon with frequency $\omega_{\mathrm{sum}} = \omega_p + \omega_s$. Under certain temperature conditions, the cascade of SFG and EO polarization coupling is achievable with one single poling period. Then, in the quantum physics, the effective Hamilton operator for the cascade process can be described by the following form [15]:

$$\hat{H} = i\hbar(\chi_1 \hat{a}_{\mathrm{sV},l} \hat{a}^{\dagger}_{\mathrm{sH},l} + \chi_2 E_{\mathrm{pH}} \hat{a}_{\mathrm{sH},l} \hat{a}^{\dagger}_{\mathrm{sumH},l} - \mathrm{H.c.}), \quad (1)$$

where $\hat{a}_i$ and $\hat{a}^{\dagger}_i$ represent, respectively, the annihilation and creation operators for the wave at frequency ω_i, with $i = s$ and sum representing signal and SFG photons, respectively. H and V represent the quantum polarization states in the horizontal and vertical directions, respectively. And l denotes the OAM index of the signal and SFG photons. Because of OAM conservation in the SFG process, the signal photon's OAM is linearly transferred during the SFG process. E_{pH} is the electric field amplitude of pump lasers. χ_1 and χ_2 are, respectively, the coupling coefficients of EO polarization coupling and SFG that are proportional to the second-order susceptibility $\chi^{(2)}$ of the crystal. In the PPLN sample, the coupling coefficient of sum frequency χ_2 is constant. H.c. denotes a Hermitian conjugate.

Considering the condition in the PPLN sample, two fundamental waves, denoted as S^e_s (single photon) and S^e_p (pump) propagate along the x direction, and the upper superscript represents the polarization direction. SFG photons (SUM^e) are generated under the condition of type-0 QPM condition. Let S^e_s also satisfy the QPM condition of transverse EO polarization coupling ($S^e_s \leftrightarrow S^o_s$). Using the Heisenberg equation of motion, the coupled-mode equations describing the cascaded processes can be obtained from Eq. (1):

$$\frac{d\hat{a}_{\mathrm{sH},l}}{dt} = \chi_1 \hat{a}_{\mathrm{sV},l} - \chi_2 E^*_{\mathrm{pH}} \hat{a}_{\mathrm{sumH},l},$$

$$\frac{d\hat{a}_{\mathrm{sV},l}}{dt} = -\chi_1 \hat{a}_{\mathrm{sH},l}, \qquad (2)$$

$$\frac{d\hat{a}_{\mathrm{sumH},l}}{dt} = \chi_2 \hat{a}_{\mathrm{sH},l} E_{\mathrm{pH}}.$$

III. EXPERIMENT AND RESULTS

In our scheme, the internal structure of the PPLN is sketched in Fig. 1. The light propagation direction is along the X axis and the Z axis is the optical axis. The dimension of PPLN is $25.0(x) \times 0.3(y) \times 1.0(z)$ mm^3. The electrodes are coated on its Y surface and connected to an adjustable voltage supplier. The poling period Λ of the PPLN is 20.65 µm at 21 °C, which is designed to fulfill the quasi-phase-matching (QPM) condition. In the theoretical calculation, the matching points satisfying the cascade condition are calculated by the Sellmeier equation [22], as shown in Fig. 1(b). Because of the relatively weak dispersion of PPLN, SFG has the same period as second-harmonic generation (SHG). The period of PPLN we use in the experiment is in accordance with theoretical simulation. When a transverse electric field is applied along the Y axis, the positive and negative domains are alternately rearranged at small rocking angles of θ and $-\theta$ of the optical axis about the x axis with the expression of $\theta \approx \gamma_{51} E / [(1/n^2_e) - (1/n^2_o)]$ [23], where E is the transverse electric field intensity, γ_{51} is the EO coefficient, and n_e, n_o are the extraordinary and ordinary refractive indices, respectively. Meanwhile, the QPM condition is determined by $\lambda = \Lambda (n_o - n_e)$ corresponding to the operating wavelength. At the QPM condition, the polarization of the output is rotated by an angle of $2N\theta$ relative to its horizontal or vertical initial state. The geometry is the same in the previous reports [24].

We first apply a polarization analyzer to carry out EO polarization coupling experiment with only S^e_s input. The experimental setup of the PPLN device for polarization control is depicted in Fig. 6 (Appendix). In polarized-coupling process, both vertically and horizontally polarized inputs exhibit the same properties. With a voltage supplier, the upper limit of electrical modulation rate for EO polarization coupling is measured to be approximately
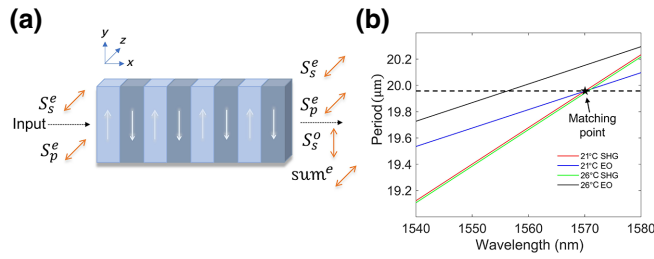
FIG. 1. (a) Schematic diagram of the cascading process. (b) The theoretical matching period of the PPLN corresponding to the cascade condition. The condition of the matching point is the period of PPLN used in our experiment.

2 MHz [24]. Figure 2 shows the experimental matching relation of EO polarization coupling, and the tuning slope is -0.76 nm/$^{\circ}$C. Then, we implement a power meter and a filter to test the QPM conditions of SFG. We inject two fundamental waves with e polarization to generate e-polarized SFG wave at the wavelength of 785.4 nm. We determine the cascade condition by interacting the EO polarization-coupled S_s^e wavelength with the pump light ($S_s^e + S_p^e \rightarrow$ SUM^e), and also find a better experimental condition at approximately 1556.6 nm at 34.5°C. The slope of linear fitting is 0.28 nm/$^{\circ}$C. This demonstrates the ability of up-conversion and efficient mode conversion for EO coupling of the PPLN device.

These characteristics of single photon with OAM modes are investigated next. Our experimental setup is shown in Fig. 3, which first describes a schematic diagram of spontaneous parametric down-conversion (SPDC) source. Light from a femtosecond laser with a repetition rate of
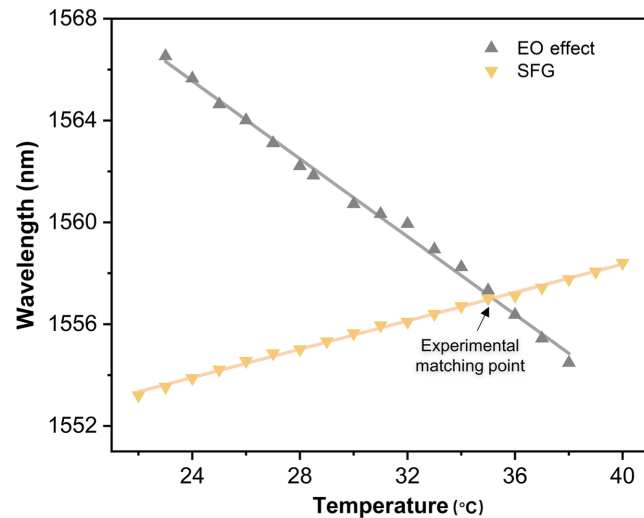

FIG. 2. Temperature tuning of EO polarization-coupled cascaded SFG processes. The intersection of the two curves is the experimental matching point.

60 MHz is separated by coarse wavelength division multiplexing (CWDM) and a filter and, respectively, amplified by two erbium-doped optical fiber amplifiers (EDFAs), which are used as signal light (International Telecommunication Union channels: CH34) and pump laser with a wavelength of 1585.3 nm (S_p^e), respectively. S_p^e is first amplified by L-band EDFA and then collimated to free space. The pulses (CH34) amplified by the EDFA are frequency doubled in a PPLN waveguide by SHG, and then the remaining pump laser is suppressed by a WDM with an extinction ratio of 180 dB. The second SH is injected to another 5-cm-long PPLN waveguide for the type-0 SPDC process to generate single photons in the communication band. We use cascaded 100-GHz dense WDM (DWDM) filters to transfer signal photons to channels with wavelengths of 1556.6 nm (CH26) and 1543.5 nm (CH42), respectively. At the output of the SPDC module, photons (CH26) with different polarizations are split into different paths by PBS-1. The single photon from CH42 is directly detected by the superconducting nanowire single-photon detectors (SNSPDs, Photec Corp.) with the detection efficiency of over 90%. To deterministically generate the topological charge of the OAM superposition quantum state, spiral phase plates (SPPs) as mode shifters are inserted into the two arms of modified MZI [25] for converting Gaussian photons to OAM-carrying photons. The diffraction efficiency of the SPPs is over 98%. In our experiments, another continuous-wave laser with a central wavelength of 1550 nm is injected into another input of the beam splitter (BS) as the feedback to perform phase-locking operation of the interferometer [26]. Then, we prepare the polarization of the quantum state with OAM mode $l = 1$ as horizontal, and when $l = -1$, the polarization of the OAM quantum state is vertical, which can generate an initial state: $|\psi\rangle_0 = 1/\sqrt{2}(|1\rangle_H + |-1\rangle_V)$. l is an integer and represents the topological charge of the photon generated with SPP. Although $l = 1$ is used in our experiment, all experimental results can be extended to other l values. Considering that the quantum state of the incident photon is the superposition of any two OAM modes l and $-l$ with opposite signs, the polarizations of signal photons with different modes are perpendicular to each other. For convenience, we denote the OAM qubit basis by $|1\rangle(|l\rangle)$ and $|-1\rangle(|-l\rangle)$. The signal photons are combined with pump laser in BS, and launched into the PPLN device for cascade process after passing the optical 4f focusing-collimation system (composed of two convex lenses L1 and L2). Here, the PPLN device includes a PPLN sample, voltage supplier, and a temperature controller at an accuracy of 0.1 $^{\circ}$C. For detecting the signal photon before (after) SFG at 1556.6 nm (785.4 nm), a lens L4 (L6) is used to image the single photon to the spatial light modulator (SLM-A/SLM-B).

To demonstrate the flexibility and adaptability of nonlinear manipulation with the OAM quantum state, we apply
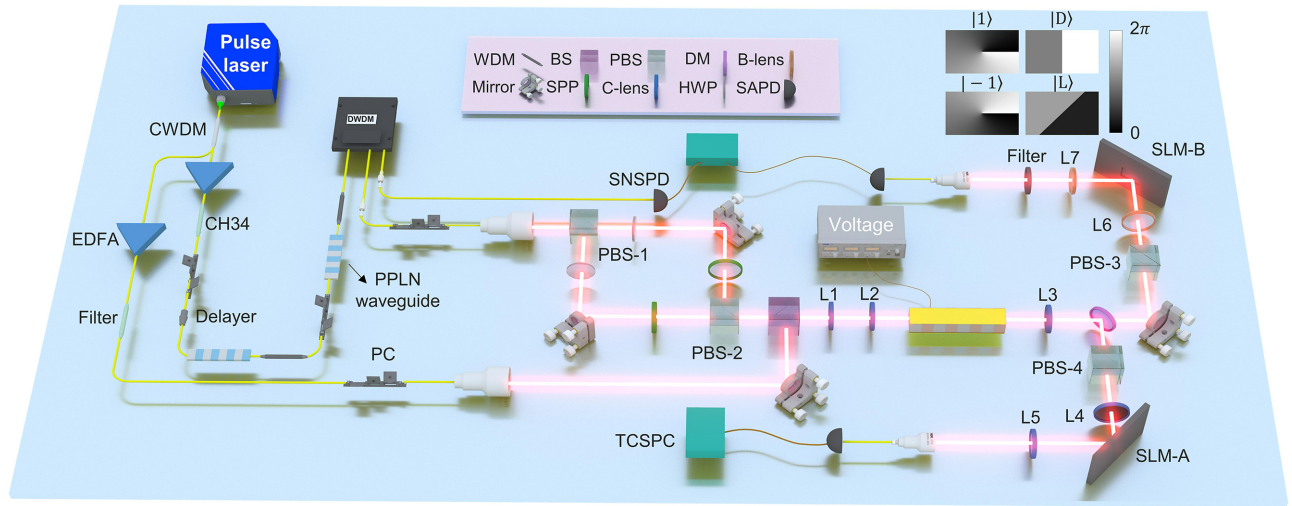
FIG. 3.   Experimental setup. HWP, half-wave plate; PC, polarization controller; L1 lens of $f_1 = 75$ mm, L2 lens of $f_2 = 40$ mm, L3 lens of $f_3 = 300$ mm, L4 and L6 lens of $f_4 = f_6 = 200$ mm, L5 and L7 lens of $f_5 = f_7 = 400$ mm; DM, dichromatic mirror; efficiency of the photon transmittance in the filter of 30%; the detection efficiency of SAPD is (50 ± 0.2)% (dark-count probability per nanosecond, $D = 1 \times 10^{-6}$).

the single photon carrying the single-mode OAM for the cascade process, and replace the structure of the interferometer with a single input of signal photons. We set the orientation of the PBS-3 (PBS-4) so that only H-polarized photons pass, and then measure the single-photon counts. The ability to control the polarization of the single photon are observed by measuring the SFG photon counts on the silicon avalanche photodiode (SAPD) under different applied voltages. The detection events of SAPD are recorded by time-correlated single-photon counting (TCSPC, ID900-mustane, Inc. Company), and the measurement window is set to 500 ps. As shown in Fig. 5(b), the SFG photon number decreases with increasing voltage because of the change of polarization of the signal photons, resulting in a decrease of SFG efficiency. To characterize the quality of frequency-correlated photon pair, we test the coincidence-to-accidental ratio (CAR) of entangled photon pairs after SFG. In the case of the pump power for the SPDC process approximately equal to 5 µW, we can obtain CAR approximately equal to 20.38. In addition, we also perform the coincidence measurements of the photon counts as a function of time delay, corresponding to Fig. 4(a). Here, the SFG photons are directly collected by the optical fiber to the SAPD. Each detection is accumulated for 10 s with the dark count subtracted. We measure the SFG efficiency of the transfer interface, when the pump power of the SFG is 20 mW, the conversion efficiency is 16%, as shown in Fig. 4(b).

Now, we characterize the performance of the SFG process by using the state $|1\rangle$ distributed on a Bloch sphere and then performing quantum state tomography (QST) before and after SFG to reconstruct the density matrix $\hat{\rho}$. In order to evaluate the $\hat{\rho}$ with four Stokes

parameters [27], projection measurements are performed on the four basis vectors $|1\rangle$, $|-1\rangle$, $|D\rangle$, $|L\rangle$, where $|D\rangle$, $|L\rangle$, respectively, represent $|D\rangle = 1/\sqrt{2}(|1\rangle + |-1\rangle)$ and $|L\rangle = 1/\sqrt{2}(|1\rangle + i|-1\rangle)$. Two spatial light modulators (SLM-A for signal photons and SLM-B for SFG photons, calibrated at wavelengths 1550 and 780 nm, respectively) are employed in combination with SAPD to characterize OAM-entangled states. Due to the restriction of QPM, the output polarization of SFG photons is the horizontal polarization state, which is also the polarization state that can be modulated by the SLM. The spiral phase front of SFG photons is then flattened to a plane wave front and converted to an Airy-like transverse pattern with most of its intensity in the center by SLM with the basis vector $|-1\rangle$, which can be efficiently coupled to a single-mode fiber. For the projection measurements of single-photon OAM quantum states, the real and imaginary parts of the density matrix $\hat{\rho}$ are experimentally reconstructed by using the maximum-likelihood estimation, as presented in Fig. 5(a). We also
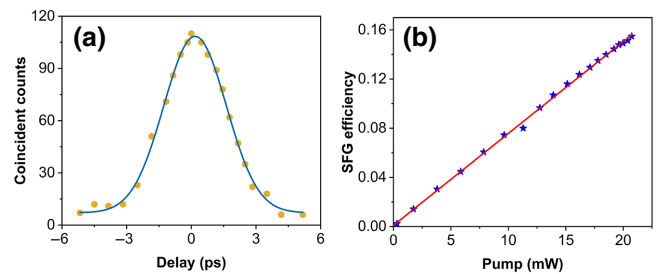

FIG. 4.   (a) The number of SFG photons versus delays of the two paths measured by SAPD. (b) Curve of SFG efficiency as a function of pump power.
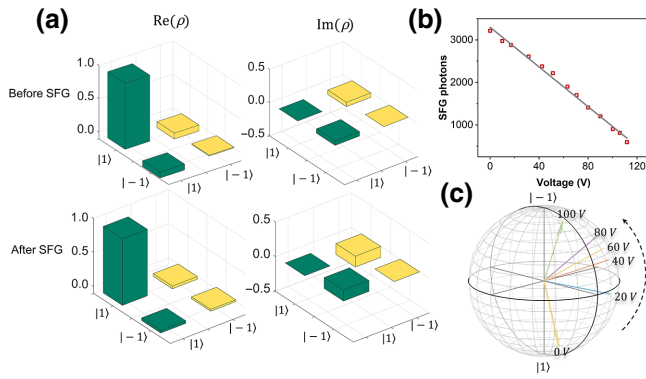
FIG. 5.　(a) The measured density matrices of the OAM states. (b) Variation trends of the number of SFG photons are recorded by varying the applied voltage with dark count subtracted. Each count is measured for 10 s. (c) Output of the OAM superposition state represented on the Poincaré sphere as the applied voltage varies from 0 to 100 V with 20-V steps.

calculate the fidelity relative to the ideal quantum state and obtain the average fidelity $F_{\text{before SFG}} = \langle\varphi|\hat{\rho}|\varphi\rangle = (98.79 \pm 0.2)\%$ and $F_{\text{after SFG}} = (97.34 \pm 0.14)\%$ with the dark count subtracted, where $|\varphi\rangle$ is the ideal quantum state. Notably, the high fidelity shows the reliable performance of the SFG in our PPLN device, thus paving the way for the realization of frequency conversion with different OAM quantum superposition states.

We further verify the manipulation capability of EO polarization coupling to transform different quantum states in the PPLN device. The initial state can be transformed into different OAM quantum superposition states via EO polarization coupling, which can be described as $|\psi\rangle = \alpha|l\rangle + \beta|-l\rangle$, where $|\alpha|^2 + |\beta|^2 = 1$, α and β depend on the EO polarization coupling effect in PPLN. We measure the transformed OAM states of the experimental output at different voltages and represent them on the Poincaré sphere, respectively, as illustrated in Fig. 5(c). As can be seen, the trajectory of quantum state evolution gradually
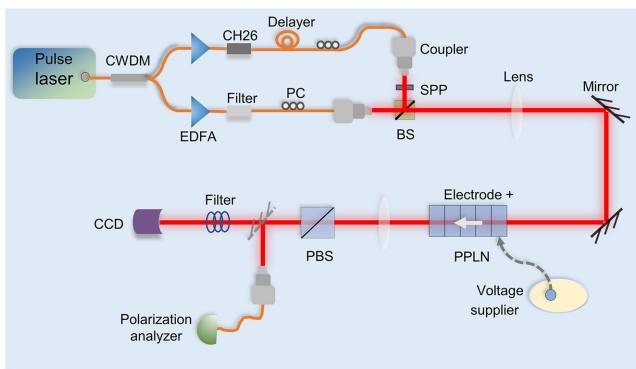
changes from the South Pole to the North Pole with respect to the increase of the applied voltage.

IV. DISCUSSION

In our experiments, the OAM states of the nonlinear process can maintain a high fidelity of over 95%. However, after frequency conversion, the fidelity of the quantum state decreases. This is mainly due to the influence of the detection efficiency of SAPD and the imperfection of optical devices, the system loss caused by the nonuniform coupling efficiency in space and fibers, which can be improved by optimizing system parameters and utilizing higher-efficiency SAPD. Compared with general waveguides, a variety of OAM modes can be transmitted in our PPLN structure, thereby realizing the switching of different modes in practical condition. It is worth noting that the key feature is the tunability of different wavelengths in the cascading scheme, which releases the constraints on the input light. This provides more flexible applications for quantum states' manipulation of quantum relay. Under classical optical conditions, l reaches 100 in the SH process [28]. If OAM states with higher topological charge would be used, the efficiency and fidelity may be degraded due to the inhomogeneity of the photon frequency conversion of the SFG process within the PPLN. If the conversion efficiency problem is solved, the size on l will not be limited. We can solve this problem by using a laser source with uniform intensity to achieve higher sum-frequency efficiency [29]. In our experiments, the OAM mode with $l = 1$ is only used as an example, which can be extended to different modes to form OAM quantum states with different l numbers in the future work. In addition, if the OAM of the pump is considered, the topological charge of the SFG photon can be controlled by the SFG interaction process between the pump and the signal photon if required. Interestingly, we hope to explore the interaction between vector structured light and the more complex vector fields of nonlinear optics, extending the frontier of electrically manipulated quantum states to different physical phenomena [29–31]. Another application is the combination of OAM-entangled quantum states and nonlinear regulation to inspire various quantum communication tasks [26]. We can construct such a state $|\Psi\rangle = 1/\sqrt{2}(|1\rangle|1\rangle + |-1\rangle|-1\rangle)$ to realize the control of entanglement-based OAM states in combination with the above-mentioned cascade process for dense-encoded quantum communication [32]. This interface can be applied to control the OAM mode of the entangled states and provides great potential applications in large-scale quantum networks.

V. CONCLUSION

In conclusion, we demonstrate a method for nonlinear manipulation of OAM quantum states by taking the advantage of the cascading process in PPLN. We successfully

FIG. 6.　Experimental setup of the cascade process.

manipulate different OAM superposition states and control the intensity of frequency conversion through the EO polarization coupling while maintaining a high fidelity. Furthermore, we expect that our scheme holds promise for realizing quantum information tasks such as superdense teleportation, dense encoding, and multinode integrated space-to-fiber communication networks.

ACKNOWLEDGMENTS

APPENDIX A: EXPERIMENTAL SETUP OF THE CASCADE PROCESS

The experimental setup is depicted in Fig. 6. Light from a femtosecond laser with a repetition rate of 60 MHz is separated by CWDM and a filter and, respectively, amplified by two EDFAs, which are used as signal light (International Telecommunication Union channels: CH26) and pump laser with a wavelength of 1585.3 nm, respectively. The signal photon is optically delayed and together with the pump wave, nonlinear processes are performed. The signal light after the spiral phase plates (SPPs) and the pump light are collimated into the free space, and then combined by the 50:50 beam splitter (BS). OAM qubits are generated with a SPP placed in the optical path. The combined beam injected into the PPLN device after passing through a lens. The output is collimated to free space by a short focal-length lens, and then captured by a silicon-based CCD in the visible band after passing a polarized beam splitter (PBS) and a filter with 150-dB isolation. Under the condition of QPM of the above SFG process, the Gaussian-mode intensity profile is imaged by a spherical lens and captured by the CCD, and we can recognize that the central intensity of the profile gradually becomes weaker with the increase of the applied voltage, as shown in Fig. 7.

APPENDIX B: INTENSITY PROFILES OF THE GENERATED SFG AND SHG WAVES

To demonstrate the electrical manipulation ability of the cascade process, we apply a voltage change to invoke EO polarization coupling and monitored the intensity change of SUM^e as shown in Fig. 7. We introduce the OAM mode of the SH waves (marked as 2ω) and SFG waves (marked
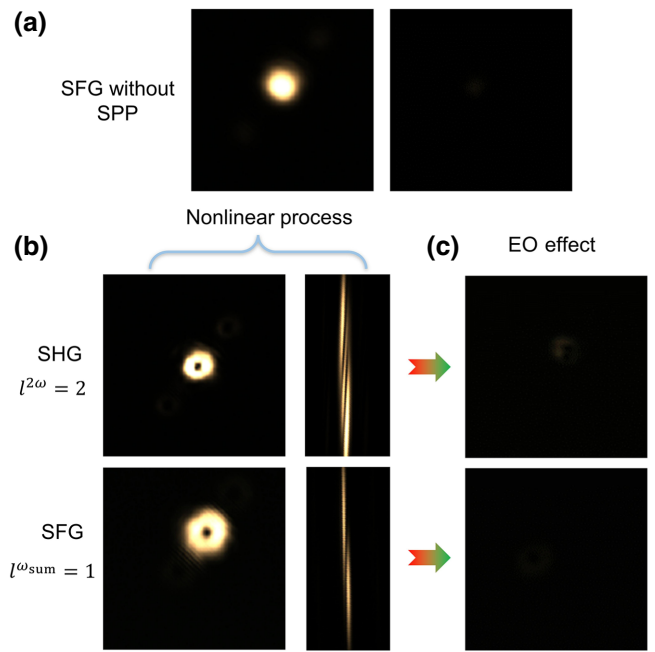

FIG. 7. (a) Intensity profiles of the generated SFG waves without SPP (left). The pattern on the right is the weakening change of the intensity with the applied voltage. (b) Intensity distribution of the generated SHG and SFG wave in the midplane of the PPLN imaged with a spherical (left) or cylindrical (right) lens during the nonlinear process. (c) Intensity profiles with increasing voltage.

as ω_{sum}) as optical states, where l is an integer and represents the photon's topological charge generated with SPP. When a Gaussian photon is transmitted through the SPP, its azimuthal phase acquires a phase factor $\exp(il\theta)$, and its profile becomes an OAM mode with respect to l. θ is the polar angle in the transverse plane. Similarly, for the SHG process, we switch the fundamental frequency light to the central wavelength at 1570 nm and then determine the temperature under QPM conditions to match the maximum nonlinear conversion efficiency. PPLN is pumped by a collimated fundamental wave with OAM state of l^ω that generates a SHG with the state of $l^{2\omega}$. Initially, as the applied voltage increases, part of the e-polarized fundamental wave becomes o-polarized wave due to the EO polarization coupling, and the intensity of SFG waves (SUM^e) gradually decreases. When the applied voltage is further increased, the energy of the o-polarized wave couples back to the e-polarized wave. As a result, the intensity of the SFG profile gradually increases. Obviously, we verify that the efficiency of the nonlinear process in PPLN is successfully controlled by the applied electric field, thus extending the method for the modulation of superposition states of single-photon OAM. Intensity profiles of the corresponding spots of the generated SHG and SFG field imaged using a spherical and cylindrical lens, respectively. Finally, the intensity profile at the midplane of PPLN can

be recorded by the CCD, as shown in Fig. 7(b) for $l^{2\omega}$ and $l^{\omega_{sum}}$. The number of dark fringes allow the magnitude of l to be determined. The drop of the intensity in the profile is sufficient to effectively demonstrate the mismatched QPM conditions for frequency conversion in combination with EO polarization coupling.

———————

[1] S. K. Liao, W. Q. Cai, J. Handsteiner, B. Liu, J. Yin, L. Zhang, D. Rauch, M. Fink, J. G. Ren, and W. Y. Liu, *et al.*, Satellite-Relayed Intercontinental Quantum Network, Phys. Rev. Lett. **120,** 030501 (2018).

[2] C. Elliott, Building the quantum network, New J. Phys. **4,** 46 (2002).

[3] A. Mair, A. Vaziri, G. Weihs, and A. Zeilinger, Entanglement of the orbital angular momentum states of photons, Nature **412,** 313 (2001).

[4] M. Erhard, R. Fickler, M. Krenn, and A. Zeilinger, Twisted photons: new quantum perspectives in high dimensions, Light Sci. Appl. **7,** 17146 (2018).

[5] M. Mafu, A. Dudley, S. Goyal, D. Giovannini, M. McLaren, M. Padgett, T. Konrad, F. Petruccione, N. Lütkenhaus, and A. Forbes, Higher-dimensional orbital-angular-momentum-based quantum key distribution with mutually unbiased bases, Phys. Rev. A **88,** 032305 (2013).

[6] X. L. Wang, X. D. Cai, Z. E. Su, M. C. Chen, D. Wu, L. Li, N. L. Liu, C. Y. Lu, and J. W. Pan, Quantum teleportation of multiple degrees of freedom of a single photon, Nature **518,** 516 (2015).

[7] Y. Zhang, M. Agnew, T. Roger, F. S. Roux, T. Konrad, D. Faccio, J. Leach, and A. Forbes, Simultaneous entanglement swapping of multiple orbital angular momentum states of light, Nat. Commun. **8,** 1 (2017).

[8] A. Nicolas, L. Veissier, L. Giner, E. Giacobino, D. Maxein, and J. Laurat, A quantum memory for orbital angular momentum photonic qubits, Nat. Photonics **8,** 234 (2014).

[9] J. Lavoie, J. M. Donohue, L. G. Wright, A. Fedrizzi, and K. J. Resch, Spectral compression of single photons, Nat. Photonics **7,** 363 (2013).

[10] Y. Shen, X. Wang, Z. Xie, C. Min, X. Fu, Q. Liu, M. Gong, and X. Yuan, Optical vortices 30 years on: OAM manipulation from topological charge to multiple singularities, Light Sci. Appl. **8,** 90 (2019).

[11] L. Allen, M. W. Beijersbergen, R. J. C. Spreeuw, and J. P. Woerdman, Orbital angular momentum of light and the transformation of Laguerre-Gaussian laser modes, Phys. Rev. A **45,** 8185 (1992).

[12] S. Tanzilli, W. Tittel, M. Halder, O. Alibart, P. Baldi, N. Gisin, and H. Zbinden, A photonic quantum information interface, Nature **437,** 116 (2005).

[13] R. Ikuta, Y. Kusaka, T. Kitano, H. Kato, T. Yamamoto, M. Koash, and N. Imoto, Wide-band quantum interface for visible-to-telecommunication wavelength conversion, Nat. Commun. **2,** 1 (2011).

[14] M. T. Rakher, L. Ma, O. Slattery, X. Tang, and K. Srinivasan, Quantum transduction of telecommunications-band single photons from a quantum dot by frequency upconversion, Nat. Photonics **4,** 786 (2010).

[15] C. E. Vollmer, C. Baune, A. Samblowski, T. Eberle, V. Händchen, J. Fiurášek, and R. Schnabel, Quantum Upconversion of Squeezed Vacuum States from 1550 to 532 nm, Phys. Rev. Lett. **112,** 073602 (2014).

[16] B. P. da Silva, W. T. Buono, L. J. Pereira, D. S. Tasc, K. Dechoum, and A. Z. Khoury, Spin to orbital angular momentum transfer in frequency up-conversion, Nanophotonics **11,** 771 (2022).

[17] T. Xiang, Q. C. Sun, Y. Li, Y. Zheng, and X. Chen, Single-photon frequency conversion via cascaded quadratic nonlinear processes, Phys. Rev. A **97,** 063810 (2018).

[18] D. Wang, T. Ding, Y. Zheng, and X. Chen, Cascaded sum-frequency generation and electro-optic polarization coupling in the PPLNOI ridge waveguide, Opt. Express **27,** 15283 (2019).

[19] Y. Tang, K. Li, X. Zhang, J. Deng, G. Li, and E. Brasselet, Harmonic spin–orbit angular momentum cascade in nonlinear optical crystals, Nat. Photonics **14,** 658 (2020).

[20] J. Wang, J. Sun, C. Luo, and Q. Sun, Experimental demonstration of wavelength conversion between ps-pulses based on cascaded sum-and difference frequency generation (SFG+ DFG) in LiNbO$_3$ waveguides, Opt. Express **13,** 7405 (2005).

[21] G. Li, S. Zhang, and T. Zentgraf, Nonlinear photonic metasurfaces, Nat. Rev. Mater. **2,** 1 (2017).

[22] O. Gayer, Z. Sacks, E. Galun, and A. Arie, Temperature and wavelength dependent refractive index equations for MgO-doped congruent and stoichiometric LiNbO$_3$, Appl. Phys. B **91,** 343 (2008).

[23] J. Wu, Y. Huang, C. Lu, T. Ding, Y. Zheng, and X. Chen, Tunable Linear Polarization-State Generator of Single Photons on a Lithium Niobate Chip, Phys. Rev. Appl. **13,** 064068 (2020).

[24] T. Ding, Y. Zheng, and X. Chen, Phase-shifted Solc-type filter based on thin periodically poled lithium niobate in a reflective geometry, Opt. Express **26,** 12016 (2018).

[25] W. Zhang, Q. Qi, J. Zhou, and L. Chen, Mimicking Faraday Rotation to Sort the Orbital Angular Momentum of Light, Phys. Rev. Lett. **112,** 153601 (2014).

[26] Y. Huang, Y. Li, Z. Qi, J. Feng, Y. Zheng, and X. Chen, A two-way photonic quantum entanglement transfer interface, npj Quantum Inf. **8,** 1 (2022).

[27] D. F. James, P. G. Kwiat, W. J. Munro, and A. G. White, Measurement of qubits, Phys. Rev. A **64,** 052312 (2001).

[28] Z. Y. Zhou, D. S. Ding, Y. K. Jiang, Y. Li, S. Shi, X. S. Wang, and B. S. Shi, Orbital angular momentum light frequency conversion and interference with quasi-phase matching crystals, Opt. Express **22,** 20298 (2014).

[29] H. J. Wu, B. S. Yu, Z. H. Zhu, W. Gao, D. S. Ding, Z. Y. Zhou, X. P. Hu, C. Rosales-Guzmán, Y. J. Shen, and B. S. Shi, Conformal frequency conversion for arbitrary vectorial structured light, Optica **9,** 187 (2022).

[30] W. T. Buono and A. Forbes, Nonlinear optics with structured light, Opto-Electron. Adv. **5,** 210174 (2022).

[31] J. Wang, F. Castellucci, and S. Franke-Arnold, Vectorial light–matter interaction: Exploring spatially structured complex light fields, AVS Quantum Sci. **2,** 031702 (2020).

[32] X. Gu, M. Krenn, M. Erhard, and A. Zeilinger, Gouy Phase Radial Mode Sorter for Light: Concepts and Experiments, Phys. Rev. Lett. **120,** 103601 (2018).